Preparation and Characterization of Hydroxyapatite/Poly(Ethylene Oxide) Nanocomposite Nanofibers

Y.Z. Zhang[1,2,*] Q. Li[1], B.C. Yi[1], B. Su[2] and A. El-Turki[3]

[1]*College of Chemistry, Chemical Engineering and Biotechnology, Donghua University, Shanghai 201620, China*

[2]*Department of Oral & Dental Science, University of Bristol, Bristol, BS1 2LY, UK*

[3]*Interface Analysis Centre, University of Bristol, Bristol, BS2 8BS, UK*

Abstract: Developing nanofillers incorporated polymer nanofibers (*i.e.*, nanocomposite nanofibers) is an effective approach to achieve functionality and efficiency in nanomaterials applications. In this paper, spindle- or needle-shaped hydroxyapatite (HA) nanoparticles with sizes of ca. 100 x 30 nm were synthesized by a wet chemical method. HA-incorporated poly(ethylene oxide) (PEO) nanocomposite nanofibers were then successfully fabricated via electrospinning aqueous solutions of HA/PEO blends with varied HA contents. Scanning electron microscope and transmission electron microscope observations indicated that if higher HA loadings (*e.g.*, 30%, 50%) were involved, the resultant fiber morphology would be affected by occurring HA aggregates along the fiber axis. The HA nanoparticles were found to aggregate discretely forming raisin-like morphology with their long axis in alignment with the fiber direction. XRD and FTIR results provide evidence of molecular interactions between the nanocrystal HA and PEO, likely because of the formation of hydrogen bondings. With this, it is believed that further development of current HA/PEO nanocomposite nanofibers, biologically mimicking the basic building blocks of the natural bone, may lead to potential applications in repairing hard tissues like bone as well as in developing efficient optoelectronic nanodevices.

Keywords: Hydroxyapatite, Poly(ethylene oxide), Nanocomposites, Electrospinning.

1. INTRODUCTION

It has been well known that the natural bone in constituent consists mainly of two components, *i.e*., the organic collagen and the inorganic hydroxyapatite (HA), in which the HA with a chemical composition of $Ca_{10}(PO_4)_6(OH)_2$ accounts for about 70% in the total mass of the bone. From a material classification point of view, the natural bone can be regarded as a natural example of biological composite or biocomposite where the ductile organic phase of collagen contributes to increase the poor fracture toughness of HA, and the inclusion of HA to collagen gives higher stability in terms of both mechanical and degradation properties. Consequently, in the past decades much attention in the community of biomaterials for bone-repairing has been focusing on developing HA-containing polymer-based biocomposites to mimic the bone composition to some extent. Apart from constituent resemblance, significant progress in understanding hierarchical structure of bone has also prompted researches on how to achieve structural biomimicking [1, 2]. For instance, recognizing that basic building blocks of bone are the nanocomposite of HA nanocrystals [3] incorporated collagen nanofibers, in the past years some researchers have paid attention to the development of nanofibrous artificial biocomposite via a prevailing electrospinning technique.

Since 1990s, electrospinning [4-7] has gained increasing prominence in the academia and industries because of its capability of producing ultrafine high surface area micro- to nano-scale fibers applicable to a wealth of fields. Among various proposed applications, using electrospun nanofibers to construct biomimetic artificial extracellular matrix (ECM) represents one of the most important paradigms in the field of tissue engineering and regenerative medicine. Specifically in the context of electrospun nanofibers for bone engineering, several HA-containing nanocomposite nanofibers, such as HA/gelatin [8], HA/poly(3-hydroxybutyrate-co-3-hydroxyvalerate) [9], HA/poly (lactic acid) (PLA) [10], HA in the blend of polycaprolactone (PCL) and collagen [11], and HA in matrix of silk/poly(ethylene oxide) PEO [12], have been produced and investigated *in vitro*. However, the polymer matrices used are primarily based on conventional biodegradable polyesters (*e.g.*, PLA, PCL), which are hydrophobic and having very limited water retention ability compared to hydrogels [13]. These will pose problems in the permeation of water, calcium and phosphate ions, metabolic products and chemical signals between the aqueous physiological environment and the biocomposite implants. Additionally, for better biomineralization it also requires

*Address correspondence to this author at the College of Chemistry, Chemical Engineering and Biotechnology, Donghua University, Shanghai 201620, China; Tel: +86-21-67792374; Fax: +86-21-6779 2647; E-mail: yzzhang@dhu.edu.cn

E-ISSN: 2312-5470/19

that the polymer matrices should possess good affinity to the calcium and phosphate ions to induce natural synthesis of HA nanocrystals within the organic phase with the abundant calcium and phosphate existed in the human body.

The objective of this work is to synthesize nano-sized HA particles and from which to fabricate a biomimicking hydrogel-forming composite nanofibers of HA/PEO through electrospinning technique. PEO is selected as an analogue of noncollageous organic phase because it is biocompatible and hydrophilic. The polar groups like OH and C-O-C can facilitate proper adhesion between the HA and PEO and form hydrogel. PEO also possesses excellent electrospinnability from its aqueous solution system, which will not only aid in electrospinning of high HA-loaded spinning solutions but also reduce toxic concerns related to organic solvents commonly used in electrospinning. Previously, sheet-form HA/PEO composites as potential bone-bonding materials to presumably allow calcification inside the hydrogel has been investigated [14]. The remarkable affinity of PEO for calcium ions had also resulted in the development of a series of bone-bonding polymers known as Polyactive®, a block copolymer composed of a PEO segment and a poly(butylene terephthalate) (PBT) [15]. A previous endeavor also demonstrated that HA nanoparticles incorporated poly(ethylene glycol) (PEG) hydrogels could significantly improve the physical and chemical hydrogel properties as well as some biological characteristics such as osteoblast cell adhesion [16]. Thus, successful fabrication of biomimetic HA/PEO nanocomposite nanofibers will be the first step for future potential applications in repairing articular cartilage and bone in a biomimicking manner, and possibly in developing efficient optoelectronic nanodevices [17].

2. MATERIALS AND METHODS

2.1. Materials

Phosphoric acid (≥85 wt% solution in water) and calcium hydroxide (> 95%) were purchased from Sigma-Aldrich, Inc. (St. Louis, MO). Poly(ethylene oxide) (PEO) with a molecular weight of 850,000 g/mol was supplied by the Sumitomo Seika Chemicals Co. Ltd. (Japan).

2.2. Synthesis of Hydroxyapatite Nanoparticles

Hydroxyapatite nanoparticles were synthesized by a wet chemical precipitation method [18, 19] based on the reaction of calcium hydroxide with orthophosphoric acid as follows:

$$10Ca(OH)_2 + 6H_3PO_4 \rightarrow Ca_{10}(PO_4)_6(OH)_2 + 18H_2O$$

In a typical synthesis process, a stoichiometric amount (*i.e.*, Ca/P molar ratio = 1.67) of orthophosphoric acid (12.4 wt%) was added dropwise at a dropping speed of 2 mL/min to the $Ca(OH)_2$ suspension under vigorous stirring. The rotation speed of the stirrer in the reaction mixture was 1200 rpm and the reaction was conducted at room temperature. After titration, the stirring was continued for 48 h and then the obtained slurry was left to ripening (ageing) for another 24 h without stirring. Finally, the white precipitate was separated from the suspension by washing with deionized water for several times to neutral pH and vacuum filtering with Corning® vacuum filter/storage bottle system, and dried in an oven at 80 °C in air. The dried samples were then used for different characterizations. Notably, HA nanoparticles precipitated for making electrospinning solution were not subjected to drying treatment. This is to prevent the synthesized nanoparticles from aggregation and to facilitate subsequent mixing of HA/PEO solution.

2.3. Fabrication of HA/PEO Nanocomposite Nanofibers

HA/PEO solutions with varied mass ratios of 1:9, 3:7, and 5:5 for electrospinning were prepared by dissolving pre-determined amounts of PEO in HA suspensions of 10 mL the synthesized and were stirred over night for better dispersion and homogenization. Electrospinning was then performed in a custom-made chamber where the spinneret made from a B-D 22G1^1/2 tip-ground-to-flat needle was mounted on an electrically insulated stand. The spinneret needle was maintained at a voltage of 8 kV by a high voltage power supply (PS/EL30R01.5-22, Glassman High Voltage, Inc.), and an aluminum plate covered with an aluminum foil (14 x 14 cm^2) under the needle at a distance of 12 cm was grounded and used as the collector. The capillary needle spinneret was connected through polytetrafluoroethylene tubing to a plastic syringe filled with 5 mL of the HA/PEO spinning solution. A constant volume flow rate of 20 μL/min was maintained using a KD Scientific syringe pump. Ambient conditions for current electrospinning process are 32.0% humidity and 24.6°C room temperature. For comparison, pure PEO nanofibers were also prepared by electrospinning a spinnable 8 wt% PEO aqueous solution.

2.4. Characterization

X-ray diffraction (XRD) patterns of different samples were recorded at ambient temperature on an X'pert Pro Diffractometer (PW3050/60, Philips, Netherlands). The samples were irradiated with monochromatized CuKα (1.5405 Å) X-ray source at a scanning rate of 0.02 °/min (2θ). The operating voltage and current used were 40 kV and 30 mA, respectively, with the beam size of 20 μm. Infrared spectra of the samples pressed into KBr disks were recorded with a Perkin-Elmer FTIR spectrophotometer at a resolution of 2 cm^{-1}. For Raman spectroscopy, sample surface was examined on normal microscopic slide at room temperature with a Renishaw InVia spectrometer using a 785 nm line of a Renishaw solid state laser. Laser beam from a strip laser diode was focused on the sample surface using a 50x objective lens into a spot of 0.5 μm x 20 μm. The laser power on the sample was about 200 mW. The spectrometer was calibrated using a monocrystalline silicon standard specimen. Images of the precipitated HA and electrospun nanocomposite fibers were obtained with a JEOL 6330F field emission gun scanning electron microscope (FEG-SEM) operated at an accelerating voltage of 10 kV. Prior to imaging, the samples mounted on aluminum stubs were platinum or carbon coated for better conductivity during imaging. Transmission electron microscopy (TEM) analysis was performed on a JEOL 1200EX electron microscope operated at 120 kV. Samples for TEM were prepared by directly depositing electrospun nanofibers onto carbon-coated 3-mm diameter copper grids.

3. RESULTS AND DISCUSSION

3.1. Synthesis of HA Nanoparticles

Several characterization techniques were performed to confirm the HA nature of the as-synthesized product. Figure **1a** shows the typical well resolved XRD pattern of the as-synthesized calcium phosphate. It matches to the JCPDS (Joint Committee on Powder Diffraction Standards No. 9-432) standard pattern for hydroxyapatite crystal and is consistent with the previous studies [20-22]. This confirms the formation of crystalline HA. It also implies that current HA was prepared at an acceptable purity because no impurity other than HA is detected from the indexed XRD pattern. Furthermore, the wide and discernable peaks also suggest that the synthesized HA has a small size and certain crystal quality. Raman spectra of the precipitated sample were presented in Figure **1b**, and was labeled in accordance with that of the HA spectrum reported [23, 24]. The strongest intensity band at 962 cm^{-1} is assigned to v1; and the peaks at the band ranges of 430-450, 580-610, and 1050-1070 cm^{-1} can be assigned to v2, v4, and v3, respectively. Whereas the band at approximate 3580 cm^{-1}, which is slightly higher than the reported 3570 cm^{-1}, could be ascribed to the OH stretching vibration mode.

Figure **2a** illustrates the FTIR spectrum of the HA nanoparticles. The spectrum shows the characteristic peaks of adsorbed water, phosphate, hydroxyl, and carbonate species. The broad peak at 3435 cm^{-1} and the relatively sharp peak at 1638 cm^{-1} correspond to the adsorbed water of the HA. The bands at 962, 1038,

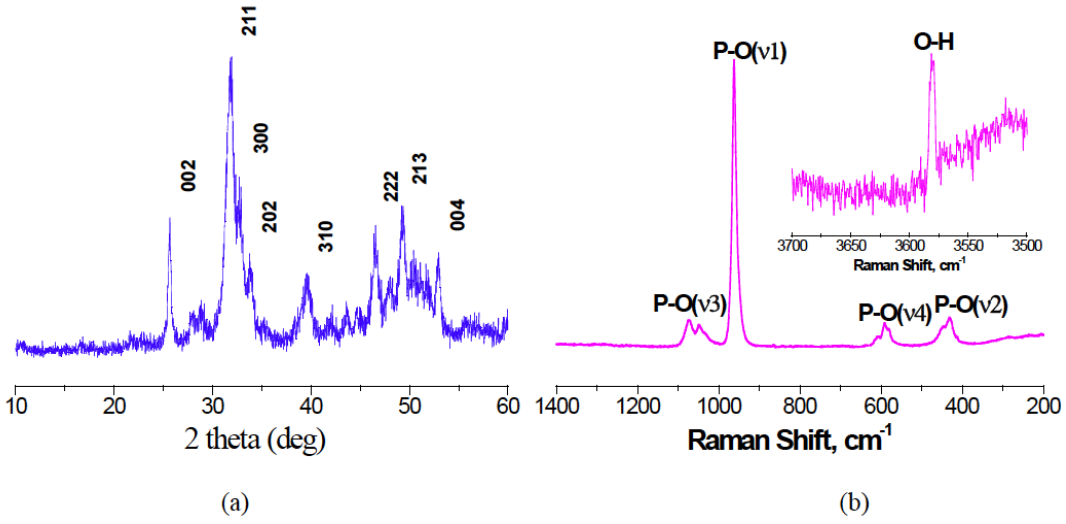

Figure 1: Typical XRD pattern (**a**) and Raman spectra (**b**) of HA precipitated at room temperature from solution with mixing ratio of Ca/P=1.67.

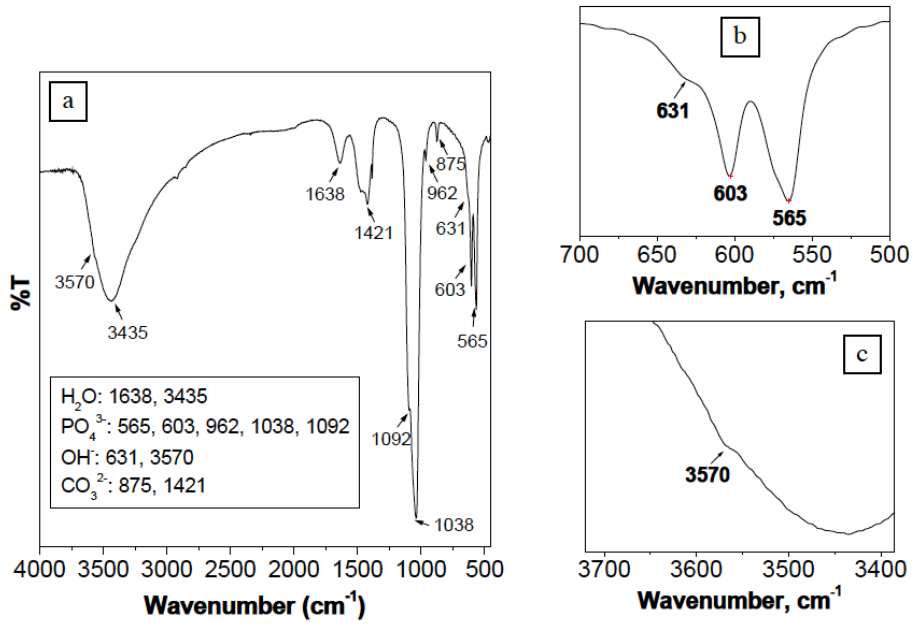

Figure 2: FTIR spectrum of the as-synthesized HA nanoparticles (**a**), and locally magnified views showing the weak OH^- bands at 631 and 3570 cm^{-1} (**b, c**) which are not clearly visible in the full spectrum (**a**).

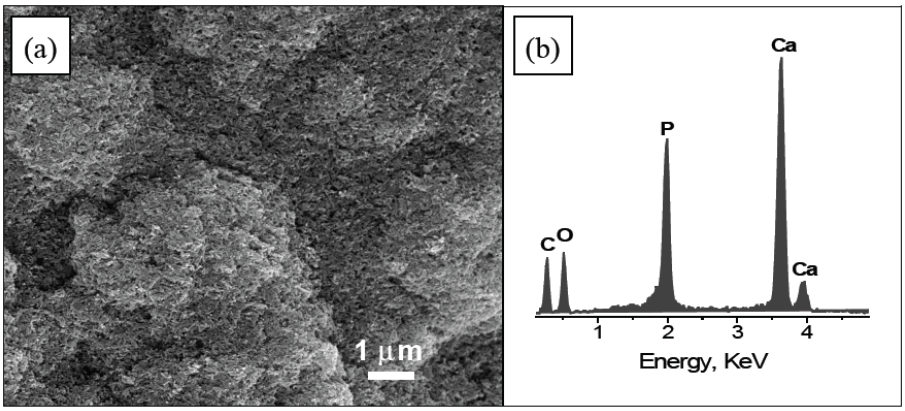

Figure 3: Scanning electron microscope photograph of HA nanoparticles showing spindle- or needle-shaped morphology (**a**), and EDX analysis of the synthesized nano HA (**b**).

and 1092 cm^{-1} are attributed to the HA PO_4^{3-} stretching vibration, and the bands at 603 and 565 cm^{-1} are due to HA PO_4^{3-} bending vibration [25, 26]. However, the identifying structural hydroxyl OH^- stretching vibration at 3570 cm^{-1} and libration mode at 631 cm^{-1} (Figure **2b,c**) are relatively weaker compared to other bands in Figure **2a**. Wet chemical precipitation at room temperature usually gives rise to lower crystallinity, which in practice results in the detection of the most characteristic OH^- mode due to the O-H bond stretching vibration at ~3570 cm^{-1} becoming difficult [22, 27, 28]. In addition, the presence of bands at 875 and 1421 cm^{-1} suggests the existence of carbonate ions CO_3^{2-} and indicates the HA a carbonated apatite. Carbonate could be introduced into the HA from the atmosphere during preparation process. Presence of carbonate ions in the wet precipitation method has been reported by many researchers [19, 29, 30]. The FTIR spectrum is consistent with those of reported in literature and is further proved that the precipitated calcium phosphate is HA.

Figure **3a** shows the FEG-SEM photograph of the synthesized HA nanoparticles, revealing that the HA nanoparticles are in the spindle- or needle-shaped morphology with a length of about 100 nm and a diameter of ca. 30 nm. The image also reveals that these nanoparticles tend to form agglomerates due to flocculation. Furthermore, the presence of Ca and P with the precipitated HA was confirmed by the energy dispersive X-ray spectrometer attached to the FEG-SEM (Figure **3b**). The presence of C in the EDX

spectrum supports the presence of carbonate groups noted in the FTIR spectrum (Figure **2a**). However, the Ca/P atomic ratio was found to be 1.54, which is slightly lower than that of the stoichiometric HA, 1.67, indicative of slight Ca-deficiency with the precipitated HA product. Calcium-deficient HA could lead to partial removal or missing of the hydroxyl groups from the lattice to balance each calcium deficiency [31], which consequently results in weaker stretching and vibrational bands compared to stoichiometric hydroxyapatite [32-34]. This also partially explains the observation of weak OH bands in the FTIR spectrum of Figure **2a**. Nevertheless, current calcium-deficient hydroxyapatite could be more useful for biological applications than stoichiometric ones because the Ca/P atomic ratio in native bone is lower than 1.67 [35]. It has been reported that calcium-deficient HA elicits an immediate precipitation of biologically equivalent apatite on its surface when immersed in a simulated physiological fluid, whereas precipitation on stoichiometric HA requires an induction time [19].

3.2. Electrospinning HA/PEO Nanocomposite Nanofibers

Nanocomposites of HA/PEO with the HA loading ratios from 10%, 30%, to 50 wt% were all electrospun into nanofibers (Figure **4b-d**). Although the electrospun fibers of HA/PEO (10% HA) (Figure **4b**) have the similar morphology as that of the electrospun pure PEO (Figure **4a**), further increasing the HA loadings not only led to fibers with irregular geometry by occurring raisin-like aggregates along the fiber axis (Figure **4c,d**), but also gave rise to decreased fiber diameters. For instance, the fiber size for the HA/PEO (30% HA loading) appeared to be 190 nm (Figure **4c**), which is thinner than that of the pure PEO nanofibers (approximately 300 nm, Figure **4a**). However, the raisin-like aggregates of HA nanoparticles along the

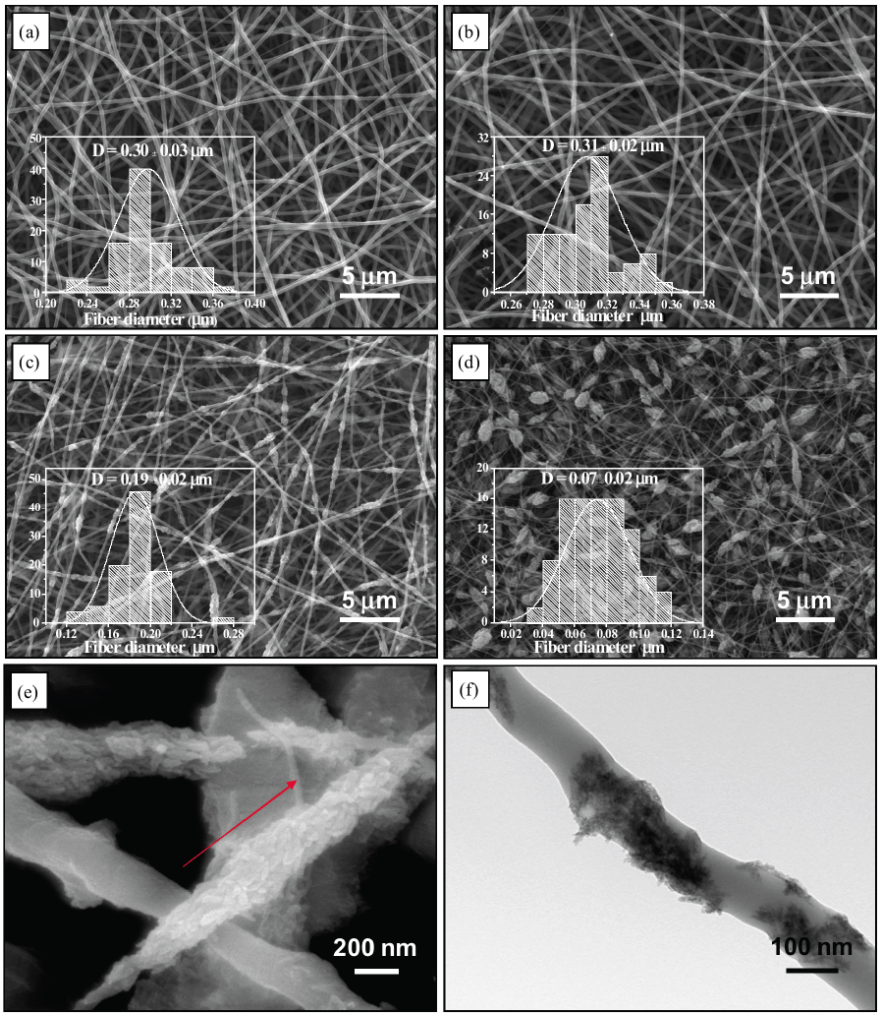

Figure 4: Scanning electron microscope photographs of the electrospun nanofibers of pure PEO (**a**), HA/PEO (10% HA) (**b**), HA/PEO (30% HA) (**c**), HA/PEO (50% HA) (**d**), HA/PEO (50% HA) at high magnification (**e**), and TEM photograph of electrospun HA/PEO (50% HA) nanofiber (**f**).

nanofiber axis (Figure **4e**) clearly suggest an inhomogeneous dispersion of the nanoparticles within the matrix PEO, even though the PEO per se could play a role in facilitating dispersion [36, 37]. PEO is the long chain form of PEG, which has been reported to be a good dispersant because PEG molecules with highly mobility, large exclusion volume, and free of charges can avoid the strong interaction between the constituents [38]. The non-uniform distribution of HA nanoparticles can also be observed from the TEM image (Figure **4f**), revealing that some segments of the nanofiber are absent of the HA nanoparticles. Although higher loading of HA nanoparticles tends to give rise to the common agglomeration problem, this study also implies that the long chain PEO could have limited dispersing ability compared with short chain PEG. To resolve this problem, *in situ* biomimetic synthesis and electrospinning might be a promising approach to explore [36]. Interestingly, it is also noted that even in the status of aggregation spindle- or needle-shaped HA nanoparticles parallel to the axis direction of the electrospun fibre is observed, suggesting better orientation effect with electrospinning. Alignment of nano-components within the electrospun nanofibers, as a result of the uniaxial extension of the fluidic jet during electrospinning process, has been similarly observed previously [39-41]. With the as-spun nanofibrous HA/PEO, insoluble nanofibrous hydrogel of HA/PEO can be obtained by radiation process [42] on the nanocomposites to make crosslinked nanofibrous HA/PEO hydrogel.

The XRD pattern (Figure **5**) of the electrospun HA/PEO nanocomposite indicates that those major characteristic peaks for both the PEO (*e.g.*, 19.0°, 23.2°) and HA at 25.7° (002), 31.9° (211), 32.9° (300), and 33.8° (202) are all present, suggesting their respective crystalline nature remains after electrospinning. It is also noted that those weak reflections appeared in pure PEO and HA are absent and the strong ones became diminished with slightly broadening. This could be associated with specific molecular interactions between them, likely resulted from the formation of hydrogen bonds between the polymer and HA crystals.

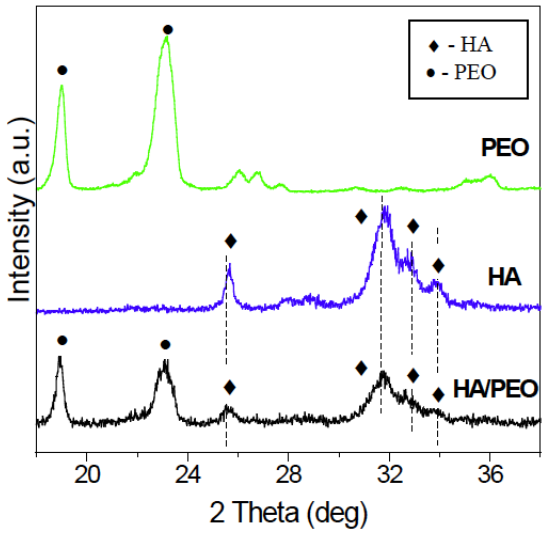

Figure 5: XRD patterns of the electrospun HA/PEO nanocomposite nanofibers, HA, and PEO.

Figure **6a** shows FTIR spectra of HA, PEO powders and their blend HA/PEO in nanofibrous form. For the spectrum of pure PEO which is in good agreement with the literature [43, 44], the two bands at 842 and 962 cm^{-1} are related to methylene group CH_2 rocking mode, and the triplet peaks at 1151, 1096 and 1060 cm^{-1} with maximum at 1096 cm^{-1} are ascribed to the stretching mode of the C-O-C group. Furthermore, the bands at 1243 and 1283 cm^{-1} are attributed to CH_2 twisting vibration, while the ones at 1342 and 1468 cm^{-1} are assigned to the CH_2 wagging and bending modes, respectively. Additionally, a large broad band of asymmetric CH_2 stretching appears between 3000 and 2750 cm^{-1} with two narrow bands at 2741 and 2695 cm^{-1}. In combination with the HA spectrum, it is found that the FTIR spectrum of HA/PEO nanocomposite nanofibers presents almost all the characteristic peaks of PEO and HA as observed in their single component counterparts, indicating the chemical characteristics of HA and PEO remain. However, it is noted that the PEO characteristic stretching vibration peak of the C-O-C at 1096 cm^{-1} shifted to 1101 cm^{-1} (Figure **6b**). Hydrogen bonding between the OH groups of HA and the etheric oxygen in the PEO molecules is proposed to be the mechanism for such a shift. In addition, there is also a slight lower frequency shift for the HA apparent band (1038 → 1035 cm^{-1}) likely due to the hydrogen bonding formation between the PO_4^{3-} groups and the residual hydroxyl end groups in the PEO, *i.e.*, HO-$(CH_2CH_2O)_n$-H. These slight shifts in the position of particular absorption bands for the PEO and HA are indicative of interactions of PEO with the HA nano-crystals. In this sense, to have good HA-PEO molecular interactions, it is necessary to introduce some smaller molecular weight PEO, *i.e.*, PEG, into the nanocomposites. This will not only facilitate to appropriate dispersing HA nanoparticles within the organic phase, but also contribute to future cross-linking effect in terms of having proper gel-strength properties.

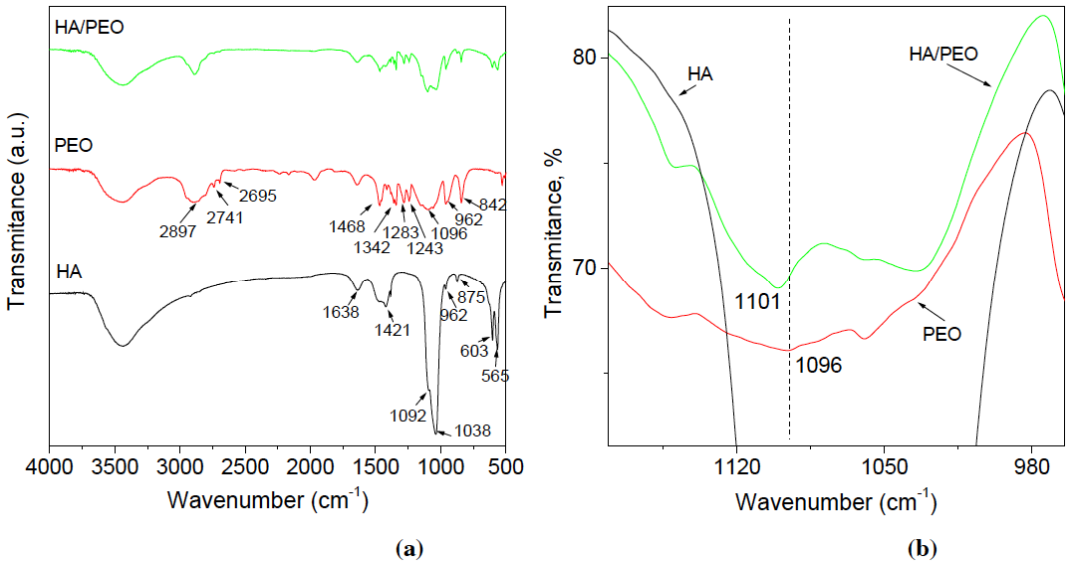

Figure 6: (**a**) FTIR spectra of HA, PEO powders and electrospun HA/PEO nanocomposite nanofibers. (**b**) C-O-C band shift from 1096 to 1101 cm^{-1} possibly due to molecular interactions between HA and PEO.

PEO as a synthetic biocompatible polymer, possesses hydrogel properties that presumably allow calcification inside the hydrogel [14]. This suggests its suitability as an appropriate polymeric matrix to compound with the hydroxyapatite nanoparticles for engineering bone tissue engineering scaffolds or bone filler with improved biomineralization capability upon implantation. A successful conversion of the HA/PEO nanocomposite into nanofibrous form would be advantageous as it enables to recapitulate the ultrastructure of the natural bone to realize structural biomimicking in bone tissue scaffold design and fabrication. In terms of the mechanical properties of PEO, although it not comparable to the widely used biodegradable polyesters (*e.g.*, PLA), it is still a tough, high crystalline polymer with a moderate tensile modulus and high elongation and strength. However, due to its water soluble attribute a prior crosslinking treatment through using gamma ray, electron beam, or chemical crosslinking is required prior to being applied for bone repair and regeneration uses. This is the subject of our future investigation towards developing insoluble nanofibrous hydrogels of HA/PEO.

4. CONCLUSIONS

In conclusion, spindle- or needle-shaped calcium-deficient hydroxyapatite nanoparticles with sizes of 100 x 30 nm were synthesized by a wet chemical approach. The XRD, Raman spectroscopy, and FTIR characterization confirmed its hydroxyapatite nature. Furthermore, nanocomposite nanofibers of HA/PEO with an averaged diameter of 200~300 nm were fabricated by means of electrospinning technique. To have better dispersion of HA within the PEO matrix, the HA loading can be controlled below 30%. It is also noted that the HA nanoparticles were aggregated discretely forming raisin-like morphology within the PEO nanofiber matrice and oriented with their long axis in alignment with the fiber direction. XRD and FTIR results provided evidence of molecular interactions between the nanocrystal HA and PEO, possibly because of the formation of hydrogen bondings. As scope of the paper is limited to the synthesis, fabrication, and characterization of the HA/PEO nanofibers, further work on radiation cross-linking of the nanocomposite nanofibers and relevant biological evaluations towards repairing hard tissue such as bone will be performed in future.

ACKNOWLEDGEMENTS

This research was supported in part by the Engineering and Physical Sciences Research Council (UK) grant, the Pujiang Talent Programme funded by the Science and Technology Commission of Shanghai Municipality (10PJ1400200), and Scientific Research Foundation for Returned Scholars (11W10523), Ministry of Education of China. Thanks are also extended to Dr. M. Li who assisted in FTIR characterization.

REFERENCES

[1] Y. Zhang, B. Su, J. Venugopal, S. Ramakrishna, CT. Lim, Biomimetic and Bioactive Nanofibrous Scaffolds from Electrospun Composite Nanofibers: A Review, Int J Nanomedicine 2007; 2(4): 1-16.

[2] JY. Rho, L. Kuhn-Spearing, P. Zioupos, Mechanical properties and the hierarchical structure of bone, Med. Eng. Phys 1998; 20(2): 92-102. https://doi.org/10.1016/S1350-4533(98)00007-1

[3] WJ. Landis, MJ. Song, A. Leith, L. McEwen, BF. McEwen, Mineral and Organic Matrix Interaction in Normally Calcifying Tendon Visualized in Three Dimensions by High-Voltage Electron Microscopic Tomography and Graphic Image Reconstruction, J. Struct. Biol. 1993; 110(1): 39-54. https://doi.org/10.1006/jsbi.1993.1003

[4] D. Reneker, I. Chun, Nanometre diameter fibres of polymer - produced by electrospinning, Nanotechnology 1996; 7(3): 216-223. https://doi.org/10.1088/0957-4484/7/3/009

[5] ZM. Huang, YZ. Zhang, M. Kotaki, S. Ramakrishna, A review on polymer nanofibers by electrospinning and their applications in nanocomposites, Compos. Sci. Technol. 2003; 63(15): 2223-2253. https://doi.org/10.1016/S0266-3538(03)00178-7

[6] D. Li, Y. Xia, Electrospinning of nanofibers: reinventing the wheel?, Adv. Mater 2004; 16(14): 1151-1170. https://doi.org/10.1002/adma.200400719

[7] A. Greiner, J. Wendorff, Electrospinning: A Fascinating Method for the Preparation of Ultrathin Fibers, Angewandte Chemie International Edition 2007; 46(30): 5670-5703. https://doi.org/10.1002/anie.200604646

[8] HW. Kim, JH. Song, HE. Kim, Nanofiber Generation of Gelatin-Hydroxyapatite Biomimetics for Guided Tissue Regeneration, Adv. Funct. Mater 2005; 15(12): 1988-1994. https://doi.org/10.1002/adfm.200500116

[9] Y. Ito, H. Hasuda, M. Kamitakahara, C. Ohtsuki, M. Tanihara, IK. Kang, OH. Kwon, A composite of hydroxyapatite with electrospun biodegradable nanofibers as a tissue engineering material, J. Biosci. Bioeng 2005; 100(1): 43-49. https://doi.org/10.1263/jbb.100.43

[10] HW. Kim, HH. Lee, JC. Knowles, Electrospinning biomedical nanocomposite fibers of hydroxyapatite/poly(lactic acid) for bone regeneration, Journal of Biomedical Materials Research Part A 2006; 79A(3): 643-649. https://doi.org/10.1002/jbm.a.30866

[11] J. Venugopal, P. Vadgama, TSS. Kumar, S. Ramakrishna, Biocomposite nanofibres and osteoblasts for bone tissue engineering, Nanotechnology 2007; 18(5): 1-8. https://doi.org/10.1088/0957-4484/18/5/055101

[12] C. Li, C. Vepari, HJ. Jin, HJ. Kim, DL. Kaplan, Electrospun silk-BMP-2 scaffolds for bone tissue engineering, Biomaterials 2006; 27(16): 3115-3124. https://doi.org/10.1016/j.biomaterials.2006.01.022

[13] KY. Lee, DJ. Mooney, Hydrogels for Tissue Engineering, Chem. Rev 2001; 101(7): 1869-1880. https://doi.org/10.1021/cr000108x

[14] R. Banat, T. Tincer, Study on the properties of crosslinking of poly(ethylene oxide) and hydroxyapatite-poly(ethylene oxide) composite, J. Appl. Polym. Sci 2003; 90(2): 488-496. https://doi.org/10.1002/app.12695

[15] P. Li, D. Bakker, CA. vanBlitterswijk, The bone-bonding polymer Polyactive(R) 80/20 induces hydroxycarbonate apatite formation in vitro, J. Biomed. Mater. Res 1997; 34(1): 79-86. https://doi.org/10.1002/(SICI)1097-4636(199701)34:1<79::AID-JBM11>3.0.CO;2-K

[16] AK. Gaharwar, SA. Dammu, JM. Canter, CJ. Wu, G. Schmidt, Highly Extensible, Tough, and Elastomeric Nanocomposite Hydrogels from Poly(ethylene glycol) and Hydroxyapatite Nanoparticles, Biomacromolecules 2011; 12(5): 1641-1650. https://doi.org/10.1021/bm200027z

[17] H. Tsutsumi, Y. Hisha, Y. Shibasaki, Hydroxyapatite-Imidazole-Polyethylene Oxide Composites as an Ionic Conductive Material, Electrochem. Solid State Lett. 8(5) (2005) A237-A239. https://doi.org/10.1149/1.1874653

[18] M. Akao, H. Aoki, K. Kato, Mechanical properties of sintered hydroxyapatite for prosthetic applications, J Mater Sci 1981; 16(3): 809-812. https://doi.org/10.1007/BF00552220

[19] A. Osaka, Y. Miura, K. Takeuchi, M. Asada, K. Takahashi, Calcium apatite prepared from calcium hydroxide and orthophosphoric acid, J. Mater. Sci.-Mater. Med 1991; 2(1): 51-55. https://doi.org/10.1007/BF00701687

[20] F. Chen, ZC. Wang, CJ. Lin, Preparation and characterization of nano-sized hydroxyapatite particles and hydroxyapatite/chitosan nano-composite for use in biomedical materials, Mater. Lett 2002; 57(4): 858-861. https://doi.org/10.1016/S0167-577X(02)00885-6

[21] LJ. Kong, Y. Gao, WL. Cao, YD. Gong, NM. Zhao, XF. Zhang, Preparation and characterization of nano-hydroxyapatite/chitosan composite scaffolds, J. Biomed. Mater. Res. Part A 2005; 75A(2): 275-282. https://doi.org/10.1002/jbm.a.30414

[22] MR. Saeri, A. Afshar, M. Ghorbani, N. Ehsani, CC. Sorrell, The wet precipitation process of hydroxyapatite, Mater. Lett 2003; 57(24-25): 4064-4069. https://doi.org/10.1016/S0167-577X(03)00266-0

[23] PN. de Aza, F. Guitian, C. Santos, S. de Aza, R. Cusco, L. Artus, Vibrational Properties of Calcium Phosphate Compounds. 2. Comparison between Hydroxyapatite and β-Tricalcium Phosphate, Chem. Mater 1997; 9(4): 916-922. https://doi.org/10.1021/cm9604266

[24] M. Weinlaender, J. Beumer, EB. Kenney, PK. Moy, F. Adar, Raman microprobe investigation of the calcium phosphate phases of three commercially available plasma-flame-sprayed hydroxyapatite-coated dental implants, J. Mater. Sci.-Mater. Med 1992; 3(6): 397-401. https://doi.org/10.1007/BF00701234

[25] A. Ślósarczyk, C. Paluszkiewicz, M. Gawlicki, Z. Paszkiewicz, The FTIR spectroscopy and QXRD studies of calcium phosphate based materials produced from the powder precursors with different CaP ratios, Ceramics International 1997; 23(4): 297-304. https://doi.org/10.1016/S0272-8842(96)00016-8

[26] A. Slosarczyk, Z. Paszkiewicz, C. Paluszkiewicz, FTIR and XRD evaluation of carbonated hydroxyapatite powders synthesized by wet methods, J. Mol. Struct 2005; 744-747: 657-661. https://doi.org/10.1016/j.molstruc.2004.11.078

[27] G. Penel, G. Leroy, C. Rey, B. Sombret, JP. Huvenne, E. Bres, Infrared and Raman microspectrometry study of fluor-fluor-hydroxy and hydroxy-apatite powders, J. Mater. Sci.-Mater. Med 1997; 8(5): 271-276. https://doi.org/10.1023/A:1018504126866

[28] PN. de Aza, C. Santos, A. Pazo, S. de Aza, R. Cusco, L. Artus, Vibrational Properties of Calcium Phosphate Compounds. 1. Raman Spectrum of β-Tricalcium Phosphate, Chem. Mater. 1997; 9(4): 912-915. https://doi.org/10.1021/cm960425d

[29] I. Yamaguchi, K. Tokuchi, H. Fukuzaki, Y. Koyama, K. Takakuda, H. Monma, J. Tanaka, Preparation and microstructure analysis of chitosan/hydroxyapatite nanocomposites, J. Biomed. Mater. Res 2001; 55(1): 20-27. https://doi.org/10.1002/1097-4636(200104)55:1<20::AID-JBM30>3.3.CO;2-6

[30] L. Zhang, YB. Li, AP. Yang, XL. Peng, XJ. Wang, X. Zhang, Preparation and in vitro investigation of chitosan/nano-hydroxyapatite composite used as bone substitute materials, J. Mater. Sci.-Mater. Med 2005; 16(3): 213-219. https://doi.org/10.1007/s10856-005-6682-3

[31] RM. Wilson, JC. Elliott, SEP. Dowker, LM. Rodriguez-Lorenzo, Rietveld refinements and spectroscopic studies of the structure of Ca-deficient apatite, Biomaterials 2005;

26(11): 1317-1327.
https://doi.org/10.1016/j.biomaterials.2004.04.038

[32] X. Deng, J. Hao, C. Wang, Preparation and mechanical properties of nanocomposites of poly(D,L-lactide) with Ca-deficient hydroxyapatite nanocrystals, Biomaterials 2001; 22(21): 2867-2873.
https://doi.org/10.1016/S0142-9612(01)00031-X

[33] Y. Li, J. Wijn, CPAT. Klein, S. Meer, K. Groot, Preparation and characterization of nanograde osteoapatite-like rod crystals, J. Mater. Sci.-Mater. Med 1994; 5(5): 252-255.
https://doi.org/10.1007/BF00122393

[34] YB. Li, CPAT. Klein, J. Wijn, S. Meer, K. Groot, Shape change and phase transition of needle-like non-stoichiometric apatite crystals, J. Mater. Sci.-Mater. Med 1994; 5(5): 263-268.
https://doi.org/10.1007/BF00122395

[35] JAS. Bett, LG. Christner, WK. Hall, Hydrogen held by solids. XII. Hydroxyapatite catalysts, J. Am. Chem. Soc 1967; 89(22): 5535-5541.
https://doi.org/10.1021/ja00998a003

[36] C. Qiu, X. Xiao, R. Liu, Biomimetic synthesis of spherical nano-hydroxyapatite in the presence of polyethylene glycol, Ceram. Int. 2007; 34(7): 1747-1751.
https://doi.org/10.1016/j.ceramint.2007.06.001

[37] J. Duan, X. Huang, E. Wang, PEG-assisted synthesis of ZnO nanotubes, Mater. Lett 2006; 60(15): 1918-1921.
https://doi.org/10.1016/j.matlet.2005.12.052

[38] Y. Fujishiro, H. Yabuki, K. Kawamura, T. Sato, A. Okuwaki, Preparation of Needle-Like Hydroxyapatite by Homogeneous Precipitation under Hydrothermal Conditions, J. Chem. Technol. Biotechnol 1993; 57(4): 349-353.
https://doi.org/10.1002/jctb.280570409

[39] Y. Dror, W. Salalha, RL. Khalfin, Y. Cohen, AL. Yarin, E. Zussman, Carbon nanotubes embedded in oriented polymer nanofibers by electrospinning, Langmuir 2003; 19(17): 7012-7020.
https://doi.org/10.1021/la034234i

[40] YZ. Zhang, Y. Feng, ZM. Huang, S. Ramakrishna, CT. Lim, Fabrication of Porous Electrospun Nanofibers, Nanotechnology 2006; 17(3): 901-908.
https://doi.org/10.1088/0957-4484/17/3/047

[41] F. Ko, Y. Gogotsi, A. Ali, N. Naguib, H. Ye, G. Yang, C. Li, P. Willis, Electrospinning of continuous carbon nanotube-filled nanofiber yarns, Adv. Mater 2003; 15(14): 1161-1165.
https://doi.org/10.1002/adma.200304955

[42] YC. Nho, Y. Mook Lim, Y. Moo Lee, Preparation, properties and biological application of pH-sensitive poly(ethylene oxide) (PEO) hydrogels grafted with acrylic acid(AAc) using gamma-ray irradiation, Radiat. Phys. Chem 2004; 71(1-2): 239-242.
https://doi.org/10.1016/j.radphyschem.2004.03.046

[43] Y. Ji, K. Ghosh, X.Z. Shu, B. Li, JC. Sokolov, GD. Prestwich, RAF. Clark, MH. Rafailovich, Electrospun three-dimensional hyaluronic acid nanofibrous scaffolds, Biomaterials 2006; 27(20): 3782-3792.
https://doi.org/10.1016/j.biomaterials.2006.02.037

[44] EM. Guerra, KJ. Ciuffi, HP. Oliveira, V2O5 xerogel-poly(ethylene oxide) hybrid material: Synthesis, characterization, and electrochemical properties, J. Solid State Chem 2006; 179(12): 3814-3823.
https://doi.org/10.1016/j.jssc.2006.08.018

Received on 24-10-2019 Accepted on 12-11-2019 Published on 6-12-2019

DOI: https://doi.org/10.12974/2311-8717.2019.07.4